NTHAS9: The Ninth Korea-Japan Symposium on Nuclear Thermal Hydraulics and Safety
Buyeo, Korea, November 16- 19, 2014

Paper Number N9P0043

NUMERICAL STUDY ON CCFL CONDITION BASED ON THIN FILM FLOW MODEL COUPLED WITH VOF METHOD

Taro Watanabe[1*], Akira Yamaguchi[1], Takashi Takata[1]

[1] Graduate School of Engineering, Osaka University
2-1 Yamadaoka, Suita, Osaka, Japan, 565-0871

** Phone, Fax, E-mail: +81-6-6879-4099, +81-6-6879-7891, watanabe_t@qe.see.eng.osaka-u.ac.jp*

ABSTRACT

Counter-current flow Limitation (CCFL) in a heat transfer tube at the SG has an influence on the core cooling under a loss of coolant accident (LOCA) in a pressurized water reactor (PWR) because no liquid flows downstream after the CCFL. In order to improve the prediction accuracy of CCFL condition by numerical simulations using the volume of fluid (VOF) method, a liquid film flow in a counter-current flow is modeled separately from the VOF simulation. The CCFL condition was investigated analytically using the condition of maximizing quantity of a liquid film with respect to void fraction and the limitation by critical thickness of a liquid film. By combining maximum quantity of a liquid film and minimum quantity of a liquid film derived from critical thickness of a liquid film, the author has developed the estimated range of falling liquid flux under the CCFL condition. Then, a two-dimensional numerical simulation of counter-current flow in a vertical pipe has been carried out by using the VOF method. As a result of the numerical simulation, the falling water fluxes were different form the quantities of injected water. However it is confirmed that the prediction accuracy of the CCFL is improved by modifying the calculated falling water flux to the range between maximum quantity of a liquid film and minimum quantity of a liquid film.

1. INTRODUCTION

A heat removal by reflux condensation of vapor at a steam generator (SG) is considered as one of the possible core cooling methods under a loss of coolant accident (LOCA) in a pressurized water reactor (PWR). In the reflux condensation, a counter-current flow is formed in a vertical section of heat transfer tube at the SG. In the heat transfer tube, the vapor generated in the core flows upward in the center, whereas condensed water flows downward along the peripheral. When the velocity of the vapor phase increases, it prevents the water from an outflow through the tube. This process is designated as a counter-current flow limitation (CCFL). The CCFL affects the cooling performance in the reactor, therefore it is essential to understand the CCFL characteristic. In particular, the CCFL condition in which the quantity of falling water becomes zero, or no liquid film flowing downstream, is quite important because of the criteria of operating limit of reflux condensation by SG.

The CCLF is also called flooding. There has been considerable research to understand the flooding correlation by experiments under the air-water condition and theoretical analysis (Wallis, 1969) (Richter, 1981) (Bharathan et al., 1983). In addition, numerical simulations for the CCFL have been carried out.

Generally, CCFL characteristic, which is correlation between a gas flux and a liquid flux in the flooding condition, is expressed by using the Wallis correlation or Wallis parameters (Wallis, 1969) which are respectively defined as follows:

$$\sqrt{j_G^*} + m\sqrt{j_L^*} = C \tag{1}$$

$$j_k^* = j_k \sqrt{\frac{\rho_k}{g \cdot D(\rho_L - \rho_G)}}, \quad (k = G, L) \tag{2}$$

where j [m/s] is the volumetric flux, j^* is non-dimensional volumetric flux, m and C are empirical constants, D [m] is the diameter of a vertical tube, g [m/s^2] is the gravity acceleration, and ρ [kg/m^3] is the density, the subscripts L and G denote the gas and liquid phases respectively.

In numerical simulation for CCFL, it is reasonable to use a volume of fluid (VOF) Method as computational resource for two-phase flow because the VOF method has general versatility which does not require the empirical equations. However, it is too difficult to depict the CCFL condition using the VOF method, because an extremely thin liquid film, which is not analyzed in the scale of the VOF method meshes, appears at the tube surface in a condition close to the CCFL. Therefore, it is efficient for improving of the

prediction accuracy of the CCFL to couple the CCFL mechanism with the VOF Method.

In this study, a liquid film flow in a counter-current flow is modeled separately from the VOF simulation. The liquid film flow model is developed by theoretical analysis of a counter-current annular flow which is modeled by Navier-stock equation adapted boundary layer approximation or momentum balance equation in the tube. Then the developed model is coupled with the VOF simulation. As a result of comparing a two-dimensional numerical simulation with experiment data (Richter, 1981), it is concluded that the prediction accuracy of the CCFL is improved using the present method.

2. LIQUID FILM FLOW IN COUNTERCURRENT FLOW

The counter-current flow in the vertical tube is considered as an annular flow. The governing equations under the steady state flow are derived from the momentum balance at the cylindrical coordinate.

2.1 Governing Equations

2.1.1 The Case of Using Navier-Stokes Equation by Boundary Layer Approximation

The counter-current annular flow model which consists of a liquid film flow is shown in Figure 1. Region (I) is a gas phase, and region (II) and (III) is a liquid film phases. δ is thickness of a liquid film, r_i is the distance of interface form the core of a tube, r_w is the radius of a tube. Even though, the position of interface varies under the flooding, the time averaged r_i and velocity of a liquid film can be thought constant when j_G^* is constant. Therefore this model is based on the limitation of the steady states flows.

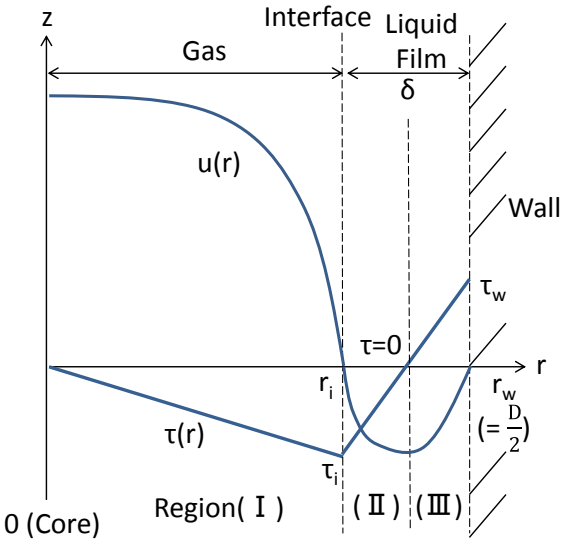

Fig. 1 Velocity profile of Counter-current annular flow model

(1) Laminar Flow

For laminar flow, a liquid film phases is not necessary to divide between region (II) and (III), the momentum equations are given as follows:

$$\frac{1}{r}\frac{\partial}{\partial r}r\mu_G\frac{\partial u}{\partial r}=\frac{\partial p}{\partial z}+\rho_G g\ ,\ (\text{gas}: 0<r<r_i) \tag{3}$$

$$\frac{1}{r}\frac{\partial}{\partial r}r\mu_L\frac{\partial u}{\partial r}=\frac{\partial p}{\partial z}+\rho_L g\ ,\ (\text{liquid}: r_i<r<r_w) \tag{4}$$

where is μ the viscosity, r is the radial coordinate, u is the velocity, dp/dz is the pressure gradient. By integrating Eq. (3) and (4) with the boundary conditions:

$\mu_G(du/dr) = 0$ at $r = 0$ and $\mu_L(du/dr) = \mu_G(du/dr)$ at $r = r_i$

following equations are given by

$$\tau=\mu_G\frac{\partial u}{\partial r}=\frac{1}{2}\left(\frac{\partial p}{\partial z}+\rho_G g\right)r\ ,$$

$$(\text{gas}: 0<r<r_i) \tag{5}$$

$$\tau=\mu_L\frac{\partial u}{\partial r}=\frac{1}{2}\left(\frac{\partial p}{\partial z}+\rho_L g\right)r-\frac{(\rho_L-\rho_G)gr_i^{\,2}}{2}\frac{1}{r}\ ,$$

$$(\text{liquid}: r_i<r<r_w) \tag{6}$$

where τ is the shear stress in counter-current flow. The velocity profiles $u(r)$ for each phase gas and liquid are determined analytically by integrating Eq. (5) and (6) with the boundary conditions:

$u = 0$ at $r = r_w$ and $u_G = u_L$ at $r = r_i$

Then by integrating $u(r)$ with respect to r at each phase, the mass flow rate of gas and a liquid film expressed by Γ are derived respectively as follows:

$$\pi D\Gamma_G=2\pi\rho_G\int_0^{r_i}ru_G dr \tag{7}$$

$$\pi D\Gamma_L=2\pi\rho_L\int_{r_i}^{r_w}ru_L dr \tag{8}$$

where Γ is related to the volumetric flux j as follow:

$$j_k=\frac{4\Gamma_k}{\rho_k D},\quad (k=G,L) \tag{9}$$

Now, the number of independent equations is two: Eq. (7) and (8), and the number of unknown variables is four, or j_G, j_L, dp/dz, and r_i. Therefore, the other two conditional equations are required in order to solve the counter-current flow model analytically.

(2) Turbulent Flow

For turbulent flow, the three layers model (Kalman, 1939) is used for introduction of the eddy viscosities,

therefore, a liquid film phases is divided between region (II) and (III). The momentum equations are similar to laminar flow: Eq. (3) and (4). However, the shear stress is given as follows, considering the eddy viscosities ε/ν:

$$\tau = \mu\left(1+\frac{\varepsilon}{\nu}\right)\frac{\partial u}{\partial r} \tag{10}$$

where ε/ν are derived from Kalman velocity profile (1939):

$$\frac{\varepsilon}{\nu} = \begin{cases} 0 & (r^+ \le 5,\ \text{laminar}) \\ \dfrac{r^+}{5} - 1 & (5 < r^+ \le 30,\ \text{transition}) \\ \dfrac{r^+}{2.5} - 1 & (r^+ > 5,\ \text{turbulent}) \end{cases} \tag{11}$$

$$r^+ = \frac{s}{\nu}\sqrt{\frac{\tau}{\rho}} = \begin{cases} \dfrac{r_i - r}{\nu_G}\sqrt{\dfrac{\tau_i}{\rho_G}} & (\tau_G < 0,\ \text{Region(I)}) \\ \dfrac{r - r_i}{\nu_L}\sqrt{\dfrac{\tau_i}{\rho_L}} & (\tau_L < 0,\ \text{Region(II)}) \\ \dfrac{r_w - r}{\nu_L}\sqrt{\dfrac{\tau_w}{\rho_L}} & (\tau_L > 0,\ \text{Region(III)}) \end{cases} \tag{12}$$

where r^+ is non-dimensional distance (Abe et al., 1991). In this case of turbulent flow, the disturbance is assumed to be generated at wall and interface. Therefore, the s in Eq. (12) is defined as distance from interface in region (I) and (II) or wall in region (III) shown in Figure 1. Then, the interface shear stress τ_i and the wall stress τ_w are determined by substituting $r=r_i$ into Eq. (5) and $r=r_w$ into Eq. (6):

$$\tau_i = \frac{1}{2}\left(\frac{\partial p}{\partial z} + \rho_G g\right) r_i \tag{13}$$

$$\tau_w = \frac{1}{2}\left(\frac{\partial p}{\partial z} + \rho_L g\right) r_w - \frac{(\rho_L - \rho_G) g r_i^{\,2}}{2 r_w} \tag{14}$$

In a similar way to the laminar flow, the mass flow rate of gas and a liquid film are given by integrating Eq. (3) and Eq. (4) with consideration for Eq. (10) respectively. In this case, the number of independent equations is two and, the number of unknown variables is four, or, j_G, j_L, dp/dz, and r_i, therefore the other two conditional equations are required in order to determine the solutions.

2.1.2 The Case of Using the Momentum Balance of Counter-current Annular Flow

In a vertical pipe, the counter-current annular flow under the steady state is shown in shown Figure 2. This model is out of considerations of the velocity profiles of gas and liquid phase. Control volume I consists of overall flow in a cross-section, and Control volume II consists of only a gas phase. Here, α is void fraction and written as $\alpha = 1-(r_i/r_w)^2$.

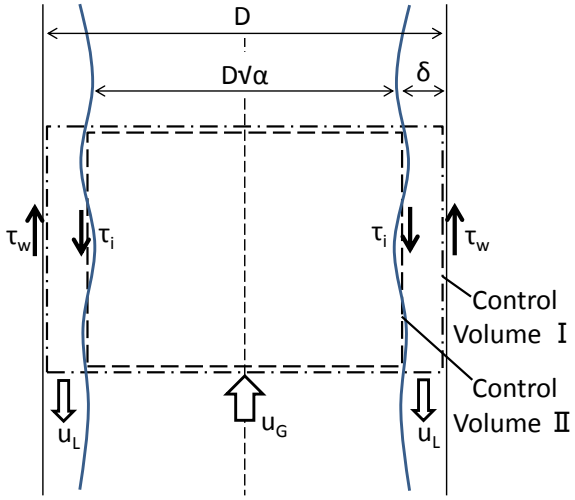

Fig. 2 Momentum balance of counter-current annular flow

The momentum balance of Control volume I is

$$-\frac{\partial p}{\partial z}\frac{\pi D^2}{2} + \tau_w \pi D - [\rho_G \alpha + \rho_L(1-\alpha)] g \frac{\pi D^2}{2} = 0 \tag{15}$$

Then, the momentum balance of Control volume II is

$$-\frac{\partial p}{\partial z}\frac{\pi D^2}{2}\alpha - \tau_i \pi D\sqrt{\alpha} - \rho_G \alpha g \frac{\pi D^2}{2} = 0 \tag{16}$$

By deleting dp/dz in Eq. (15) and Eq. (16), the governing equation is given as follow:

$$\frac{4\tau_i}{D\sqrt{\alpha}} + \frac{4\tau_w}{D} - (\rho_L - \rho_G)(1-\alpha) g = 0 \tag{17}$$

Eq. (17) is satisfied not only in a laminar flow, but also in a turbulent flow. In Eq. (17), the interface shear stress τ_i and the wall stress τ_w (Monde, 1995) are given as follows:

$$\tau_i = \frac{1}{2} f_i \rho_G (u_G + u_L)^2 = \frac{1}{2} f_i \rho_G \left(\frac{j_G}{\alpha} + \frac{j_L}{(1-\alpha)}\right)^2 \tag{18}$$

$$\tau_w = \frac{1}{2} f_w \rho_L u_L^{\,2} = \frac{1}{2} f_w \rho_L \frac{j_L^{\,2}}{(1-\alpha)^2} \tag{19}$$

where f_i is the interfacial friction coefficient, f_w is the wall friction coefficient. By using Eq. (2), Eq. (18) and Eq. (19), Eq. (17) is transformed into

$$\frac{2 f_i}{\alpha^{5/2}}\left[j_G^* + \frac{\alpha}{(1-\alpha)}\left(\frac{\rho_G}{\rho_L}\right)^{1/2} j_L^*\right]^2 + \frac{2 f_w}{(1-\alpha)^2} j_L^{*2} - (1-\alpha) = 0 \tag{20}$$

Here, the number of unknown variables is five, or, j_G, j_L, α, f_i and f_w in Eq. (20). Therefore, the other four conditional equations are required in order to solve Eq. (20).

2.2 Conditional Equations of CCFL

2.2.1 Maximum Quantity of a Liquid Film

The counter-current flow expressed in the prior section has infinite flow patterns, because the number of unknown variables is larger than of independent equations. In the prediction of CCFL, it is important to estimate the value of j_L under the condition of given j_G. If j_G is given, the number of required conditional equations is one in Eq. (7) and Eq. (8), and three in Eq. (20). We assigned empirical correlations to the coefficients: f_i and f_w, in Eq. (20) in this study therefore the number of required conditional equations is also one in Eq. (20).
Sudo (1994) reported that when j_G is constant, the CCFL condition is given by the condition that j_L becomes the maximum value as follow:

$$\frac{\partial j_L}{\partial \alpha} = 0, \ or \ \ \frac{\partial j_L}{\partial r_i} = 0 \tag{21}$$

This condition is derived from an envelope proposed by Bharathan, D. et al. (1983). He reported that an envelope of governing equation of counter-current flow gives the condition of initiate flooding.
By adapting Eq. (21) to Eq. (7) and Eq. (8), and Eq. (20) as the conditional equation, the number of required conditional equations is satisfied.

2.2.2 Interfacial Friction Coefficient and Wall Friction Coefficient

The governing equation using the momentum balance of counter-current annular flow: Eq. (20) contains the interfacial friction coefficient f_i and the wall friction coefficient f_w as unknown variables. Here, f_i and f_w are given by the following equations given by Sudo (1994) or by Wallis (1969). Sudo reported that the analytical result of j_G and j_L by using following equations fitted well the experiment data (Richter, 1981). In Sudo equations, the interfacial friction coefficient f_i is

$$f_i = 0.008\left\{1 + m \cdot \left(\frac{\delta}{D}\right)^n\right\} \tag{22}$$

$$n = 1.63 + 4.74 / Bo$$

$$m = 41.3 Bo^{(n+0.25)} \cdot 10^{9.07/Bo}$$

$$Bo = \left\{(\rho_L - \rho_G) \cdot g / \sigma\right\}^{1/2} \cdot D$$

where σ is the surface tension. Bo is non-dimensional number. The wall friction coefficient f_w is

$$f_w = A \cdot \mathrm{Re}_L{}^B \tag{23}$$

$\mathrm{Re}_L < 2000$ (Laminar): $A = 16.0, \ B = -1.0$

$2000 \le \mathrm{Re}_L < 4000$ (Transition)

$: A = 1.76 \times 10^{-10}, B = 2.32$

$\mathrm{Re}_L \ge 4000$ (Turbulent): $A = 0.314, \ B = -0.25$

Wallis obtained following equation of f_i from the experiment data of co-current annular flow. In Wallis equation, the interfacial friction coefficient f_i is

$$f_i = 0.005 \cdot \left(1 + 300 \cdot \frac{\delta}{D}\right) \tag{24}$$

Similar to Sudo equations, Eq. (23) is used as the wall friction coefficient f_w in this case.

2.3 Analytical Results and Discussions

By solving simultaneous equations of Eq. (7) and Eq. (8) or Eq. (20) and Eq. (21), j_G and j_L are determined. Considering that the liquid film flow model is coupled with the VOF method, it is acceptable for the liquid film flow model not to contain empirical correlations. Therefore Eq. (7) and Eq. (8) using Navier-stokes equation by boundary layer approximation have more benefit than Eq. (20) which contains empirical correlations. In this section, analytical results are compared with each condition.

2.3.1 The Case of using Navier-Stokes Equation by Boundary Layer Approximation

In the case of laminar flow and turbulent flow, the analytical result of j_G and j_L by using Eq. (7) and Eq. (8) with Eq. (20) is shown in Figure 3. Calculated values of j_G and j_L are greater than the experimental values. In laminar flow, the values of j_G and j_L are much greater than in turbulent flow. Additionally, diameter of a pipe is larger, j_G and j_L are lager. However the values of j_G and j_L in laminar flow are completely different from the actual value, by introduction of turbulent flow effect, j_G and j_L are mitigated and get close to the experiment data. Though in turbulent flow, j_G and j_L are also overestimated, because the interface in counter-current annular flow model shown in Figure 1 is smooth. In actual CCFL, interfacial wave is generated and the interface shear stress f_i is more effective. Therefore, the liquid film flow approaches to free fall due to the lack of l the interface shear stress. Particularly in laminar flow, diameter of a pipe is larger, the quantity of falling liquid is lager because the viscosity is small and the liquid velocity is accelerated. In order to improve calculated values of j_G and j_L, it is necessary to consider that effect of interfacial area concentration.

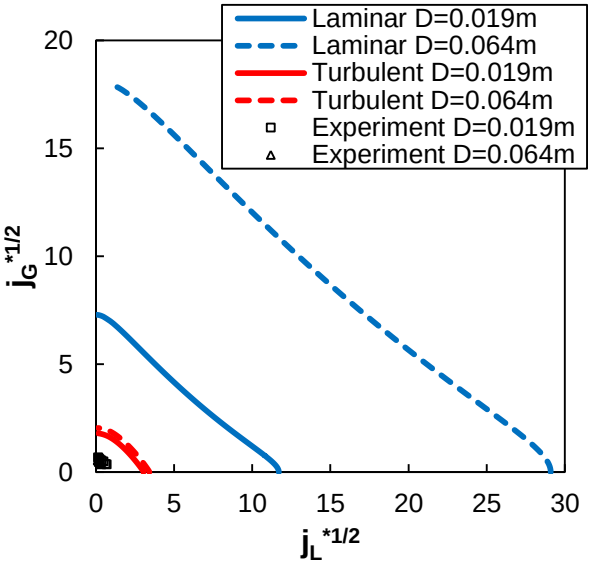

Fig. 3 Comparison of laminar flow and turbulent flow with Navier-stokes equation by boundary layer approximation

2.3.2 The Case of Using the Momentum Balance of Counter-current Annular Flow

The analytical result of j_G and j_L by using Eq. (20) with Eq. (21) is shown in Figure 4. Turbulent flow case is the result of the prior case. The result with Sudo equations was close to the experiment data. In the range of large j_G and small j_G where there is no experiment data (Richter, 1981), the experiment data is assumed to be the liner which is predicted with Eq. (1). The comparison of the liner from experiment data, the result with Sudo equations did not fit in small j_G, and in the case of D=0.019 m, the value of j_G at liquid film j_L = 0 was overestimated. In the result with Wallis equation j_G and j_L were overestimated thoroughly. It is thought that Wallis equation cannot be adjusted to the CCFL condition because Wallis equation is generated from the experiment date of co-current flow. Additionally, the result with Sudo equations only depicted the diameter size effect which the diameter is lager, the value of j_G at liquid film j_L = 0 is smaller in experiment data.

The result of liquid film thickness δ at gas flux is shown in Figure 5. Liquid film thickness becomes smaller with the increasing gas flux. In Sudo equations, liquid film thickness was the most smallest. In Wallis equation, the value of non-dimensional liquid film thickness δ^* is same as D = 0.019 m and D = 0.064 m.

The result of the interface shear stress τ_i and the wall shear stress τ_w at gas flux (D = 0.019m) is shown in Figure 6. Here, the sign of the interface shear stress in turbulent flow case of using Navier-stokes equation by boundary layer approximation is reversed. As to wall shear stress, τ_w in Sudo equation was smaller because j_L is smaller than other case. All wall shear stress peaks at j_G = 0 and decreases with the increasing gas flux. The change tendency of the wall shear stress is similar. On the other hand, the interface shear stress τ_i in Sudo equations peaks at j_G = 0. However the interface shear stress in Wallis equation and turbulent flow case of using Navier-stokes equation by boundary layer approximation are close to zero at j_G = 0, and pass through the extreme value and then decrease with the increasing gas flux.

The result of turbulent flow case of using Navier-stokes equation by boundary layer approximation may be expected to have the similar characteristic to Wallis equation.

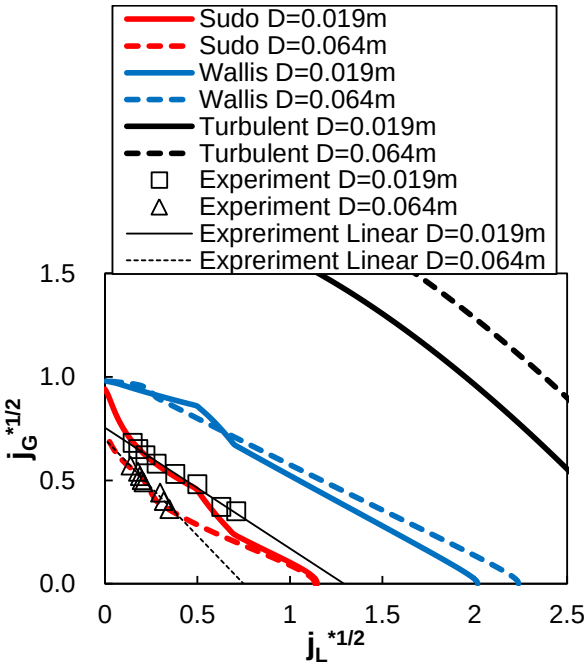

Fig. 4 Comparison of gas flux j_G and liquid flux j_L using Eq. (20)

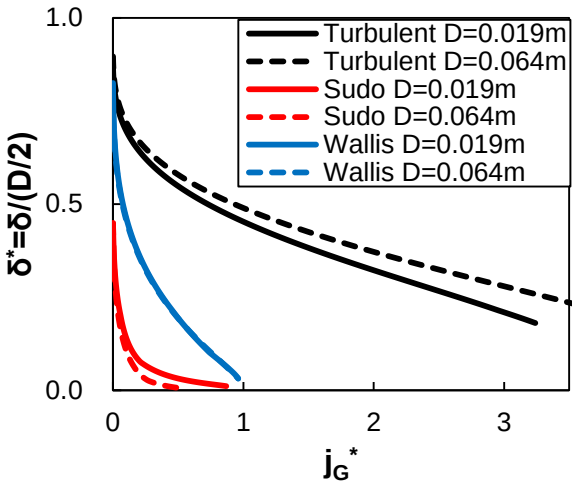

Fig. 5 Comparison of liquid film thickness δ

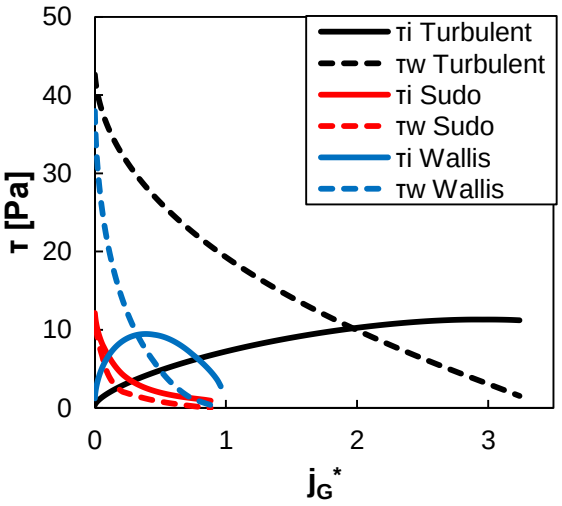

Fig. 6 Comparison of interface shear stress τ_i and wall shear stress τ_w (D = 0.019 m)

2.4 Critical Thickness of a Liquid Film and CCFL Estimation

The liquid film thickness δ and the void fraction α or r_i have correlations: $\alpha = (1-2\delta/D)^2$ or $r_i = D/2-\delta$. The calculated liquid film thickness δ may be less than physical limit in some cases. The criteria of liquid film thickness δ_{min} are evaluated by Ito (1896) as follow:

$$\delta_{\min} = 4.54 \cdot \left(\frac{g}{\nu_L^{\,2}} \right)^{-1/3} \qquad (25)$$

The result of liquid film thickness (D=0.019 m) with Sudo equations is shown in Figure 7. The result of j_G and j_L with Sudo equations was close to the experimental data. However, the value of j_G at j_L = 0 was overestimated because j_L was calculated in the range where liquid film thickness is smaller than critical thickness of a liquid film δ_{min} shown in Figure 7.

Therefore if calculated δ is less than δ_{min}, we assume that δ and j_L equal to zero because there may be no liquid film in physical process. Additionally, Eq. (21) gives the condition of "maximum" quantity of a liquid film. On the other hand, "minimum" quantity of a liquid film is given by using the condition that δ is constantly equal to δ_{min} instead of Eq. (21). It is thought that liquid flux j_L under the existence of a liquid film is estimated in the range between "maximum" quantity of a liquid film and "minimum" quantity of a liquid film. The result with above theories is shown in Figure 8. By introduction of the criteria of liquid film thickness, the value of j_G at j_L = 0 was mitigated.

In Wallis equation and the case of using Navier-stokes equation by boundary layer approximation, we cannot use above theories because calculated δ shown in Figure 5 is larger than δ_{min}.

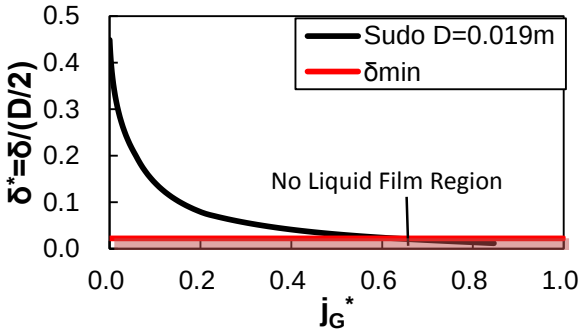

Fig. 7 Critical Thickness of a Liquid Film δ_{min}

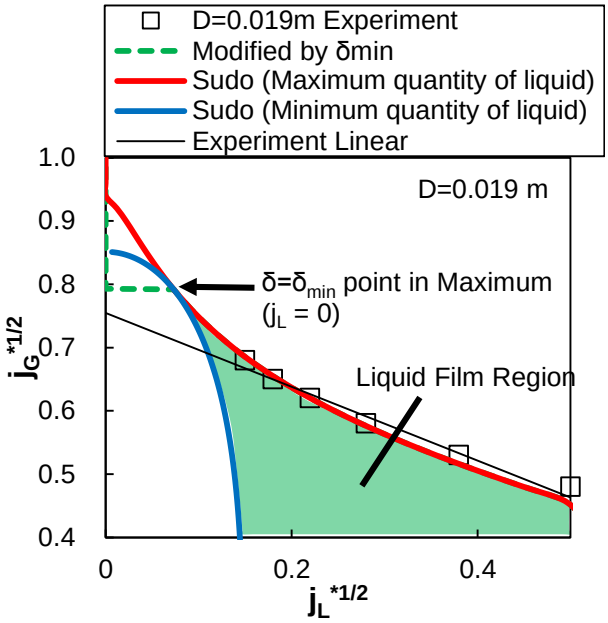

Fig. 8 Estimated range of falling liquid film flux

3. NUMERICAL ANALYSIS OF CCLF

The previous study (Murase et al., 2012) showed that the numerical simulation for the CCFL by using the VOF method was effective for the evaluation of the influence by differences between physical properties. In this study, the CCFL under the air-water condition is subject phenomenon. However, for the numerical simulation for vapor-water CCFL in actual SG, the VOF method may be a valid method because of changes of the physical properties.

3.1 Coupling the Liquid Film Flow Model with VOF Methods

We can estimate liquid flux range under CCFL by using the conditions of maximum quantity of a liquid film and minimum quantity of a liquid film. Here, as maximum condition, the analytical result of j_G and j_L obtained by the simultaneous equations of Eq. (20) and Eq. (21) with Sudo equations is used. As minimum condition, the analytical result of j_G and j_L obtained by Eq. (20) with Sudo equations and $\delta = \delta_{min}$ is used. When calculated values j_L at input value of j_G is larger than maximum quantity of a liquid film, j_L is modified to maximum j_L. Meanwhile, when j_L at injected value of j_G is smaller than minimum quantity of a liquid film, j_L is modified to minimum j_L. Additionally, when calculated liquid film

thickness δ is smaller than Eq. (25), then we assume j_L = 0.

3.2 Analytical Conditions

A two-dimensional numerical simulation of counter-current flow is carried out by using the VOF method. The numerical analysis code with the VOF is in-house, uses PLIC (Piecewise Linear Interface Calculation) to consider the interfacial gradient (Rider et al., 1998) and uses the CSF (Continuum Surface Force) model (Brackbill et al., 1992) to calculate a surface tension. The analytical model is shown in Figure 9, which a finite difference with a structural mesh arrangement in Cartesian coordinates is applied. The inner diameter D of the pipe was 0.02 m, which corresponds to the diameter of U-tubes in an actual SG. The pipe length L was 0.5 m. In the previous experiment (Kusunoki et al., 2014), the CCFL characteristic do not be affected by L when the length is over 0.3 m. In order to decrease the calculating time, the mesh is arranged roughly. The surface cells of wall of the pipe are 1.0×10^{-3} m in a horizontal direction, which is one order of magnitude larger than the critical thickness of a liquid film (around 2.0×10^{-4} m). In a vertical direction, the cells are 1.0×10^{-2} m. The time step was around 10^{-4} sec under this calculation. When injected air is $j_G^* = 1.0$ (j_G =12.7 m/s) which is sufficiently large for the CCFL in Figure 8, the distance of air moving is 1.3×10^{-3} m per one time step. It is sufficiently less than the mesh size in a vertical direction. Flow field was laminar. The pressure was 0.1 MPa and the boundary condition of constant pressure was used at the outlet. The temperature is 20°C. The surface tension σ is 0.0728 N/m and the contact angle is 45°. The air is injected to lower tank by the constant velocity boundary and flows to the pipe. The water is injected from the wall of the pipe by the constant velocity boundary in order to prevent CCFL at upper inlet of the pipe and simulate that water condenses in the SG. The falling water flux is calculated from the flow rate of water entering into the lower. The supplied water volumetric flux was constant at $j_{L,in}$ = 0.11 m/s ($j_{L,in}^{*1/2} = 0.5$) or $j_{L,in}$ = 0.44 m/s ($j_{L,in}^{*1/2} = 1.0$). The other boundaries are non-slip condition.

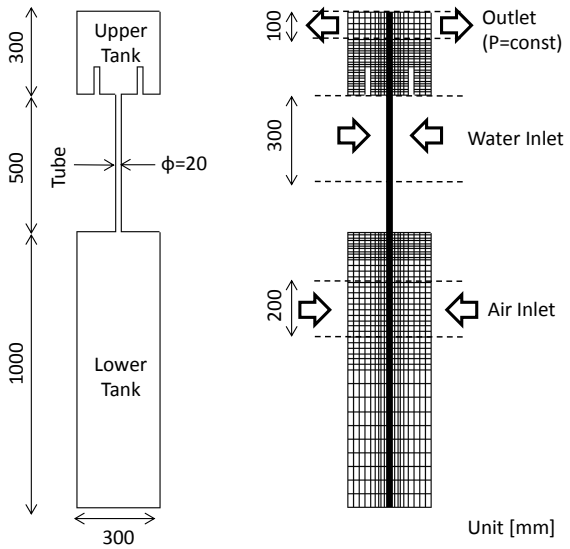

Fig. 9 Analytical model and mesh arrangement

3.3 Result and Discussions

The calculated falling water flux j_L at injected value of j_G by the VOF simulation is shown in Figure 10 ($j_{L,in}$ =0.11 m/s) and Figure 11 ($j_{L,in}$ =0.44 m/s). Modified falling water flux j_L in the range between maximum and minimum quantities of a liquid film from calculated j_L using VOF is also shown in Figure 10 ($j_{L,in}$ =0.11 m/s) and Figure 11 ($j_{L,in}$ =0.44 m/s). In both figures, the results by the VOF simulation showed that the value of $j_G^{*1/2}$ at liquid film $j_L^{*1/2} = 0$ was $j_G^{*1/2} = 0.6$ which is smaller than experimental data. In the range $j_G^{*1/2} > 0.6$, the VOF simulation calculated $j_L^{*1/2} = 0$, or there is no liquid film flow. However $j_L^{*1/2}$ increased by modifying $j_L^{*1/2}$ in the range between maximum and minimum quantities of a liquid film. The value of $j_G^{*1/2}$ at liquid film $j_L^{*1/2} = 0$ was improved to $j_G^{*1/2} = 0.8$. Therefore, in the range $j_G^{*1/2} > 0.6$, which the liquid film thickness is smaller than the critical thickness of a liquid film δ_{min}, the CCFL was mitigated.

In the range $j_G^{*1/2} < 0.5$, $j_L^{*1/2}$ increases with increasing of injected water flux $j_{L,in}$. In case $j_{L,in}$ = 0.11 m/s, $j_L^{*1/2}$ is underestimated from experiment data, but calculated $j_L^{*1/2}$ is not modified because of excessing minimum quantity of a liquid film. In case $j_{L,in}$ = 0.44 m/s, j_L^* at $j_G^{*1/2} = 0.5$ is modified because of excessing maximum quantity of a liquid film.

The flow patterns visualized by liquid fraction are shown in Figure 12. It was confirmed that CCFL was formed. In the case of $j_G^{*1/2} = 0.5$, the CCFL was generated through the pipe because the interface of liquid film was globally rough. Though, at $j_G^{*1/2} = 0.75$, laminar and smooth liquid film was formed and the CCFL was generated at lower outlet of the pipe because falling liquid film was limited thoroughly. Theses numerical analyses are carried out under two-dimensional and laminar flow condition therefore we should be pay attention to these limitation.

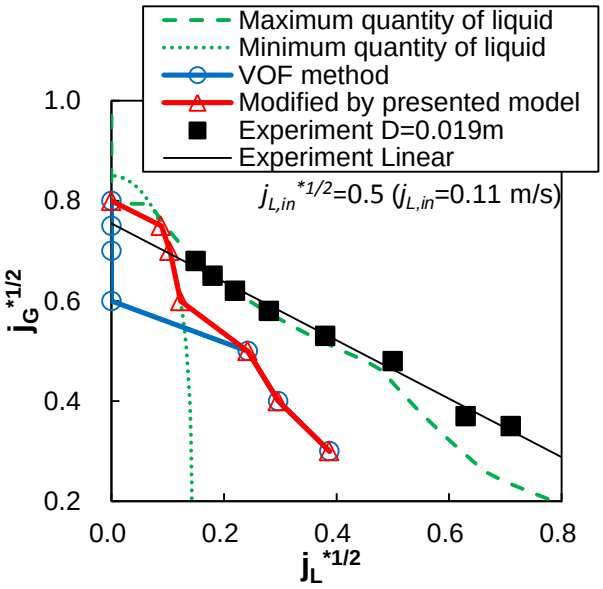

Fig. 10 CCFL characteristics by VOF simulation and modified falling liquid flux j_L by presented CCFL estimation ($j_{L,in}$ =0.11 m/s)

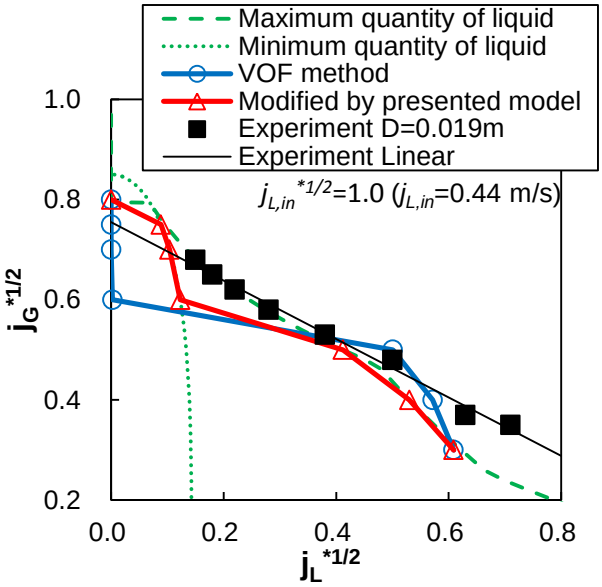

Fig. 11 CCFL characteristics by VOF simulation and modified falling liquid flux j_L by presented CCFL estimation ($j_{L,in}$ =0.44 m/s)

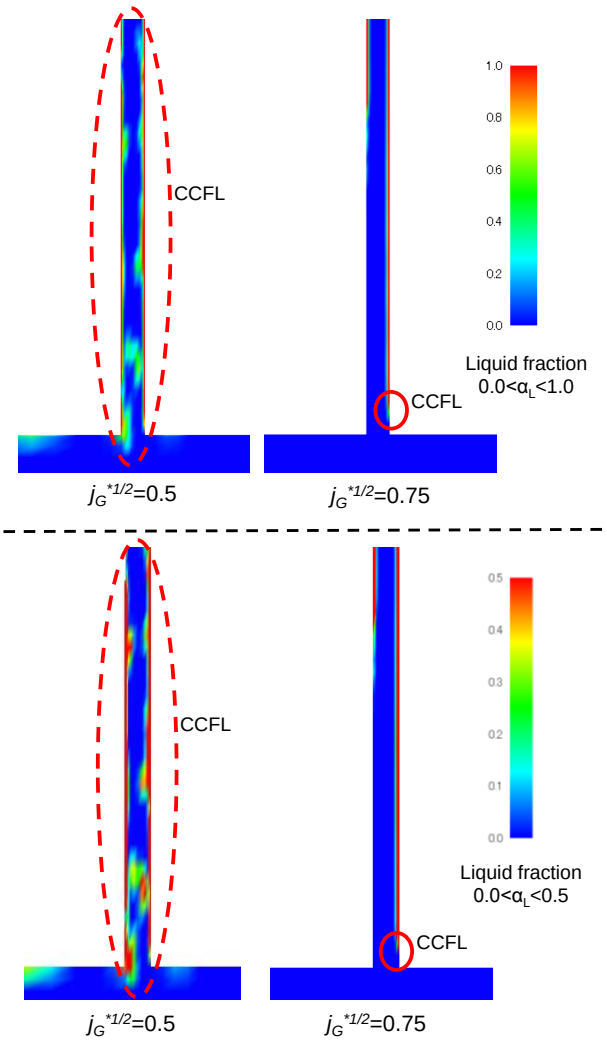

Fig. 11 Flow patterns by VOF simulation ($j_{L,in}$ = 0.11 m/s), using liquid fraction range of 0.0-1.0 for the uppers and of 0.0-0.5 for the lowers

4. CONCLUSION

In this present study, at first, a liquid film flow in a counter-current flow is modeled in order to improve the prediction accuracy of the CCFL condition by the VOF method. In the modeling of a liquid film, the analysis of the CCFL model in a vertical pipe has been done. The simultaneous equations of the momentum balance of counter-current annular flow and the condition of maximizing quantity of a liquid film with respect to void fraction using friction coefficients by Sudo(1994) have given close solutions to the experiment data. Additionally, by considering of critical thickness of a liquid film, the value of j_G at liquid film j_L = 0 has been improved. It is also possible to estimate the range of liquid flux under the CCFL condition. In the case of using Navier-stokes equation by boundary layer approximation, which does not require friction coefficients, the values of gas and liquid flux are extremely overestimated from the experiment data.

Then, a two-dimensional numerical simulation of counter-current flow in a vertical pipe has been carried out by using the VOF method. The falling water fluxes were different form the quantities of injected water. However it is confirmed that the prediction accuracy of

the CCFL, in the range $j_G^{*1/2} > 0.6$, which the liquid film thickness is smaller than the critical thickness of a liquid film δ_{min}, is improved by limiting the calculated falling water flux to the range between maximum quantity of a liquid film and minimum quantity of a liquid film.
In the future work, the authors are planning to couple the developed liquid model with the VOF method considering unsteady state.

NOMENCLATURE

j	volumetric flux	[m/s]
j^*	non-dimensional volumetric flux	[-]
D	diameter	[m]
r	radius	[m]
r^+	non-dimensional radius	[-]
s	distance from source of disturbance	[m]
p	pressure	[Pa]
f	friction coefficient	[-]
Re	Reynolds number	[-]
A	constant	[-]
B	constant	[-]
B_o	constant	[-]
n	constant	[-]
m	constant	[-]

Greek Letters

ρ	density	[kg/m^3]
δ	liquid film thickness	[m]
Γ	mass flow rate	[kg/m/s]
μ	viscosity	[Pa·s]
ν	dynamic viscosity	[m^2/s]
ε	eddy viscosity	[m^2/s]
τ	shear stress	[Pa]
α	void fraction	[-]
σ	surface tension	[N/m]

Subscripts

G	gas phase
L	liquid phase
i	interface
w	wall

REFERENCES

Abe, Y. et al. (1991). "*Estimation of Shear Stress in Counter-Current Annular Flow*," Journal of NUCLEAR SCIENCE and TECHNOLIGY, **28**(3), pp. 208-207.

Bharathan, D. et al. (1983). "*Air-Water Countercurrent Annular Flow*," Int. J. Multiphase Flow, **9**(4), pp. 349-366.

Brackbill, et al. (1992). "*A Continuum Method for modeling Surface Tension*," Journal of computational physics, 100, pp. 335-354.

Ito, A. et al. (1986). "*Breakdown and Formation of a Liquid Film Flowing down an Inclined Plane (1st Report, Measurement of Contact Angle and Mechan ism of Film Formation),*" Transactions of the JSME Ser. B, **52**(475), pp. 1261-1265.

Karman, T. (1939). "*The analogy between fluid friction and heat transfer,*" Trans. ASME, 61, pp. 705-710.

Kusunoki, T. et al. (2014). "*Air-Water Tests on Counter-current Flow Limitation at Lower End of Vertical Pipes Simulating Lower Parts of Steam Generator U-tube*," Journal of J. Multiphase Flow, **28**(1), pp. 62-70.

Monde, M. (1995). "*Analysis of Critical Heat Flux in Two-Phase Thermosyphon* (*Relationship between Maximum Falling Liquid Rate and Critical Heat Flux*)," Transactions of the JSME Ser. B, **61**(591), pp. 4101-4108.

Murase, M. et al. (2012). "*Correlation for countercurrent flow limitation in a PWR hot leg*," Journal of Nuclear Science and Technology, **49**(4), pp. 398-407.

Richter, H. J. (1981). "*Flooding in Tubes and Annuli*," Int. J. Multiphase Flow, **7**(6), pp. 647-658.

Rider, W.J. et al. (1998). "*Reconstructing Volume Tracking*," Journal of computational physics, 141, pp. 112-152.

Sudo, Y. (1994). "*Analytical Study of Critical Heat Flux under Countercurrent Flow Limitation in Vertical Channels*," Transactions of the JSME Ser. B, **60**(580), pp. 4222-4228.

Wallis, G. B. (1969). "*One-dimensional Two-phase Flow*," McGraw Hill, pp. 320-339.